Numerical Evaluation of Trabecular Bone Alterations: A Cell Method Application

Francesca Cosmi[*]

Abstract: Bone tissue is a complex multi-scale material and its morphological and functional characteristics are influenced during one's life by constant changes, physiological and pathological. A recent technique can classify the mechanical response of trabecular bone by simulating the application of loads with a Cell Method model derived from plane radiographic images of the proximal epiphyses in the patient's hand fingers, thus complementing the individual assessment with a low cost exam. The mesoscale pathological modifications (i.e. due to osteoporosis) can be detected and quantified, despite the simplification due to the use of radiograms. In this work, this approach is validated using four idealized structures, modelling different trabecular organizations in the site of interest. Then, the results obtained in six female subjects, age between 35 and 77, are discussed to highlight the potential relevance of this application for the study, in quantitative terms, of the trabecular bone alteration due to age, pathological conditions and lack of exposure to physiological mechanical stimuli (micro-gravity conditions).

Keywords: Bone quality, Cell Method, Fracture risk, Osteoporosis, Structure Index, Trabecular bone.

1   Introduction

Bone tissue is a complex multi-scale material and its morphological and functional characteristics are influenced during one's life by constant changes, both physiological and pathological. Osteoporosis represents a major health threat of important social impact: it has been estimated to affect about 200 million people worldwide, 80% of which are women [1,2]. After the age of 65 the incidence rate of hip fracture doubles every 5 years, and it can be anticipated that 30% of women and 20% of men over age 50 will suffer from an osteoporosis-related fracture during their remaining lifetime [3,4,5]. Mortality due to osteoporotic fractures has been estimated as high as 5% in the acute phase and 15-25% within one year [6]. Motor

---

[*] DIA, University of Trieste, Trieste, Italy. E-mail: cosmi@units.it

disabilities affect over 50% of patients in the year following the fracture, with 20% becoming permanent incapacities [7] and over 60% of the previously independent individuals become partially or completely dependent [8,9].

To make things worse, possibly half of people who think they are affected by osteoporosis are not at risk, while half of those actually suffering from it are not aware. Many women experiencing a fragility fracture are not appropriately diagnosed and treated [10,11]. The social and economic importance of osteoporosis is dramatically huge. Osteoporosis is, in effect, a "silent disease" with no specific symptoms. Bone deteriorates without warning signs until it becomes so weak that an unexpected knock or a fall can origin a fracture. Dual Energy X-ray Absorptiometry (DEXA) is currently the golden standard for measuring Bone Mineral Density (BMD). The DEXA test results are stated in the form of T-score, which expresses the number of standard deviations below the average BMD of the young Caucasian adult of the same gender. A T-score above -1 is considered normal, one between -1 and -2.5 is classified as osteopenia (low bone mass) and a T-score score below -2.5 indicates osteoporosis. But despite the importance of assessing the bone mineral content, it has been shown that more than half of the fragility fractures affects individuals who do not fall within this definition and the majority of fractures take place in post-menopausal women and elderly men with osteopenia, not osteoporosis [12,13,14,15]. The use of BMD as a single diagnostic method has long shown to be problematic, since studies have proved a significant overlap in BMD between osteoporotic and healthy subjects [16]. Over the years, the definition of osteoporosis has gradually shifted form a disease "of low bone density" to the one "of high bone fragility" [17]. A number of studies have been conducted in order to develop patient models for individual fracture risk assessment. These studies, of which FRAX® and QFracture® are the main examples, combine several clinical risk factors and, in some cases, BMD measurements [18,19]. It should be noted that the risk factors taken into account and the results obtained might vary from one "calculator" to the other and that their use in supporting treatment decisions is still under investigation.

It is widely recognized that the macroscale mechanical properties of the bone cancellous component depend on two factors: its composition and the complex micro-architectural quality of the trabecular arrangement. It is commonly accepted that mineral content and trabecular architecture contribute together to bone tissue overall mechanical strength. [20,21,22,23,24,25,26].

A recently introduced technique intended to provide the physician with an easy, inexpensive and fast complementary tool, evaluates the mechanical response of the trabecular structure by means of a subject-specific Cell Method model of the bone architecture obtained from a conventional X-ray image and can be combined with

the other methods for a more accurate assessment of the patient's bone quality, [27].

The technique discussed in this work assumes a simplification of the trabecular structure from 3D to 2D and can only be applied in suitable anatomic regions, such as the proximal epiphysis of the fingers of the hand, where the trabecular structure pattern develops mainly in layers and can be identified in a planar radiogram despite the irregularities of the bone shape. The *in silico* results are summarized in a Structure Index (*SI*), which removes the normalized sum of grey tones, indicative of the mineralization content, from the elastic response of the structure modeled from the radiographic image. A first initial validation on a limited number of subjects showed the potential of this tool for bone quality evaluation in osteopenic and osteoporotic patients [28]. More recently, the test provided a quantitative assessment of the bone micro-architecture pathological alterations in a case of CRPS - Complex regional Pain Syndrome type II – complicated by osteoporosis [29], showing that this procedure is able to quantify the degree and to monitor the course of bone diseases and the effectiveness of therapies.

In this work, the technique is applied to various idealized models of trabecular structure in order to substantiate the simplifications adopted and to highlight the potentialities of the Structure Index as a parameter capable:

- of grasping the differences among 3D structures despite being calculated by 2D models obtained from plain radiograms of specific anatomical sites;

- of ranking the trabecular structures on the basis of their ability to withstand the applied loads.

An example illustrating the relevance of this technique for a quantitative assessment of alterations in the human trabecular bone architectures is discussed in Section 5.

2   Method

2.1   Cell Method

The Cell Method is a recent numerical method that derives from a discrete formulation of the balance equations of physical laws [30,31,32,33,34]. The CM results generally agree with or are more accurate than those obtainable with other widely used methods such as the Finite Element Method, Finite Difference Method and Finite Volume Method. However, the Cell Method concept is deeply different from that of the mentioned methods, and brings some advantages with it. One of the major drawbacks of FEM and the other methods is that the description of a real solid will be accurate only if the field varies slowly over the size of the elements used [35]. This drawback directly originates from the use of a differential formulation of the physical laws: the field equations are then subjected to restrictions imposed

by derivability, but these restrictions are a consequence of the mathematical formulation of the method and are not related to the physics of the problem being investigated.

In effects, there is no need to write balance for a point – the node – introducing restrictions for differentiability, when balance holds also for a whole region – a discrete region – namely the influence region of the node so that the balance equation can be directly expressed in finite terms. The differences between the Cell Method and the (for some aspects similar) Finite Volume Method are discussed in [30].

A wide source of works on the Cell Method is available from the website http://www. discretephysics.org/ens/ (accessed April 17, 2015), to which the interested reader is referred.

Going into the details of the Cell Method is beyond the purpose of this paper, but it should be pointed out that one of the advantages of the Cell Method discrete approach is that no numerical device is needed when the variables cannot be differentiated or the displacement field undergoes large variations. Thus, the size of the heterogeneities in the model can be of the same order of magnitude as the discretization dimensions, effectively reducing the computational requirements to estimate the effective properties of porous solids with random voids [31,36,37] and of heterogeneous multi-phase materials, either of industrial [38,39,40] or of biological nature [41,42,43].

2.2 *Bone alterations assessment*

The procedure starts from a planar radiographic image of the hand, Fig.1(a) and investigates in silico the elastic properties of the bone tissue structure. The proximal finger epiphysis, Fig.1(b), in particular, is characterized by a trabecular pattern that develops in layers, recognizable in digital radiograms. The Region Of Interest (ROI) is selected as the largest square portion of cancellous architecture within the examined epiphysis, Fig.1(c).

Successively, the ROI image is processed and converted into a Cell Method micromechanical model, according to the procedure described in detail in [27,28,29] and briefly recalled here. A sub-threshold erosion non-linear filter is applied and a grid of nodes is placed on the ROI image. Then, the connectivity of the triangular 3-nodes cells is defined, with larger cells being used over regions of the same grey tone. The average grey tone computed in 7 points of each cell – barycentre, vertexes and sides middle points – scales the elastic modulus value in each cell from 0 MPa, for cells with no mechanical characteristics, to 1000 MPa, assumed value for the trabecular phase, Fig.1(d). A 0.3 value of Poisson's coefficient and an elastic-linear isotropic constitutive law are adopted in all the cells.
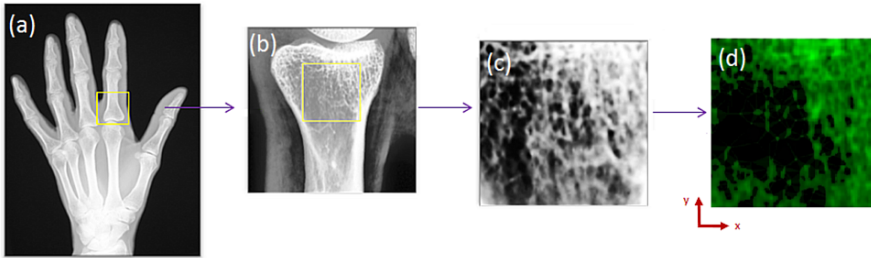
Figure 1: (a) Hand radiogram, (b) ROI selection within the proximal epiphysis, (c) ROI selected for the structural analysis, (d) pictorial representation of elastic modulus distribution.

The Cell Method micro-mechanical simulations yield the apparent elastic moduli *Ex**, *Ey** in the directions of the ROI axes and compute the Content Factor, *CF*, normalized sum of the ROI grey tones, indicative of the level of mineralization. The ability of the trabecular spatial organization to withstand the loads can be highlighted by the Structure Index *SI*, which removes the contribution of the mineralization level, related to *CF*, from E^*, average value of the apparent elastic moduli in the two directions:

$$SI = a_1[b_1 \cdot E^* - b_2 \cdot CF] \tag{1}$$

where a_1 is a normalization factor computed from the radiogram acquisition parameters, and b_1 and b_2 are positive constants. The complied code runs in the IDL Virtual Machine, a free multi-platform utility designed to provide a simple way to distribute IDL applications (http://www.exelisvis.com/docs/VirtualMachineApplicationsIntro.html accessed April 17, 2015). The entire process, inclusive of image elaboration, mesh creation and numerical computations, is completed in less than one minute on a standard notebook.

It can be pointed out that, as a general rule, the bone quality recognized by the structural index in clinically positive subjects differs from the risk identified on the basis of densitometry measurements. An example is given in Fig. 2, that plots the *SI* against the DEXA hip T-score for the 12 clinically positive subjects of the small trial partially discussed in [28].

Of the subjects, 7 were diagnosed with osteoporosis (femoral neck T-score smaller than - 2.5 SD) and 5 with osteopenia (femoral neck between -1 SD and -2.5 SD). Fig.2 highlights how the two parameters, BMD and *SI*, look at different aspects of bone fracture risk, the DEXA bone mineralization assessing the mineral content, the Structure Index quantifying the elastic load bearing capabilities of the trabecular configuration.
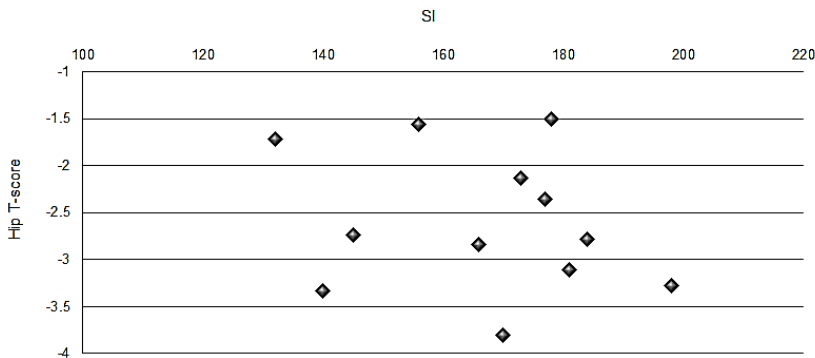
Figure 2: Structure Index *SI* vs DEXA hip T-score for 12 clinically positive sub-jects.

3   Idealized models of bone structure

While a 2D model cannot accurately predict the elastic behavior of a 3D structure, the patented method used to establish the elastic modulus distribution in the numerical model [27] does not neglect the local thickness differences in the X-rays direction. The *SI* formulation is introduced to amplify these differences, thus providing an ideal tool for bone structure quality ranking.

The ideal condition to prove this point would be a study comparing the elastic behavior of the trabecular architecture in the ROI, reconstructed by 3D CT scans, with the mechanical properties obtained from modeling the corresponding planar radiographic images. Since the required data-set has not been available yet to the Author, in this work four different idealized, out-of-scale models of the trabecular structure in the anatomical site of examination were employed to validate the use of the Structure Index for an accurate classification of trabecular architectures.

3.1   Three-dimensional idealized models

Fig.3 shows the three-dimensional simplified models (A, B, C, D) of the trabecular structure in the ROI of four different subjects. The idealized, out-of-scale, trabecular structure models dimensions are 12x12x5 mm^3. An homogeneous material with elastic modulus E=1000 MPa and Poisson ratio v=0.3 is assumed for the bone phase. It is noted that with these assumptions the bone volume fraction of the 3D structures coincides with the corresponding 2D models content factor *CF*.

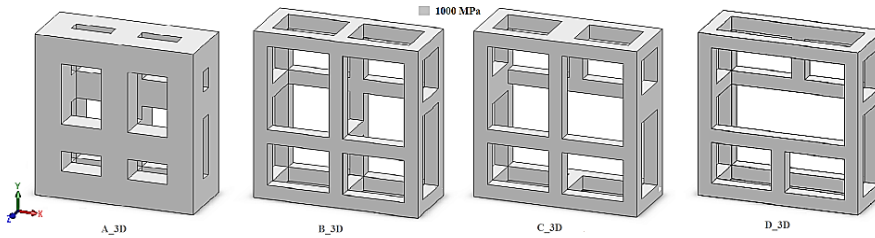As already mentioned, the trabecular structure of the hand develops in layers in

Figure 3: 3D simplified, out-of-scale, trabecular models. The structures B_3D and C_3D exhibit different resistance to the applied loads despite being characterized by the same apparent density.

the proximal epiphysis. Accordingly, the simplified model A_3D in Fig.3 consists of two square frames joined by 5 trabeculae in the z direction and by two pairs of orthogonal trabeculae, one per layer, rigidly connected to the frames. In this out-of-scale model, the trabeculae thickness is 2 mm. The content factor of model A_3D is $CF = 0.65$. Assuming a density of 2 g/cm^3 for the bone phase [44], the apparent density of the structure represented by the model A_3D amounts to 1.3 g/cm^3, which is in line with the data reported in literature for the healthy trabecular bone [45]. Subsequent models represent altered trabecular structures, for example due to osteoporosis. Model B_3D (Fig.3) has a structure similar to that of model A_3D, but the trabeculae thickness is halved to 1 mm, the structure volume fraction becomes $CF = 0.21$ and the corresponding apparent density is 0.43 g/cm^3. Model C_3D (Fig.3) is specifically designed to show the *SI* capability to discriminate among structures of the same density. The structure of A_3D was eroded in the central area until the values of *CF* of model C_3D were the same as those of B_3D but in a changed trabecular configuration and with a consequent different load bearing capability in the two structures. In the case of model D_3D (Fig.3), the volume fraction was further decreased to $CF = 0.18$, which corresponds to an apparent density of 0.37 g/cm^3. With respect to the model A_3D, both the central area and the peripheral zone were altered by creating two large holes and by removing a few trabeculae in the z direction.

Compressions along the *x* and *y* axes shown in Fig.3 were simulated. In a first series of simulations, an uniformly distributed load of 1000 N was applied. In a second series of simulations, a relative displacement of 1 mm was imposed and the apparent elastic modulus was obtained, coherently with the procedure used to compute the *SI*.

3.2   Two-dimensional idealized models

The radiographic images of the 3D structures represented in Fig.4 show different shades of grey corresponding to changes in the X-ray absorption path along the *z* direction. Coherently, the planar models corresponding to the four 3D trabecular structures, obtained with the procedure described in Section 3, are shown in Fig.4. The local level of mineralization controls the local elastic modulus to be used in the simulations. Load and boundary conditions in the simulations are analogous to those of the 3D models.
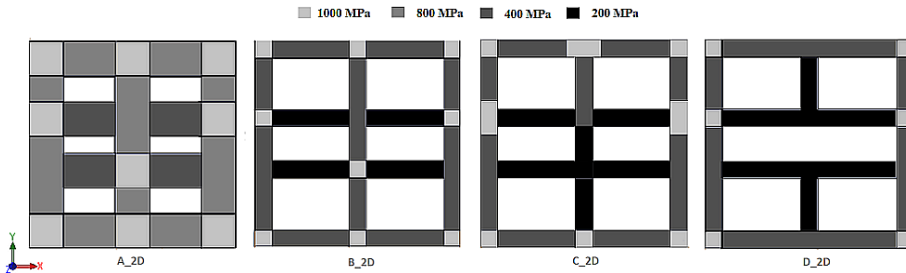
Figure 4: 2D models corresponding to the 3D out-of-scale trabecular structures in Fig.3.

4   Results

The different structures exhibit different strain and stress distributions in the controlled load simulations. For all structures, Fig. 5 shows the distribution of the equivalent strain:

$$ESTRN = \sqrt{\frac{4}{6}\left[(\varepsilon_1 - \varepsilon_2)^2 + (\varepsilon_2 - \varepsilon_3)^2 + (\varepsilon_3 - \varepsilon_1)^2\right]} \qquad (2)$$

where ε_1, ε_2, and ε_3, represent the principal strain components.

The distributions of the first principal stress and of the von Mises equivalent stress are shown in Fig. 6 and Fig. 7 for compressions in the *x* and the *y* directions respectively. As expected, the models A_3D, the healthy trabecular structure, and D_3D, the most compromised structure, are respectively the least and the most stressed. It can also be appreciated that the models B_3D and C_3D, despite being characterized by the same volume fraction and apparent density, exhibit different levels of peak stress due exclusively to the changes in the spatial configuration of the trabeculae. Notably, the general behavior exhibited by the 2D models is remarkably similar to that of the corresponding 3D models.

In the second set of simulations, the apparent elastic modulus in the directions of controlled displacement, Ex^* and Ey^*, and their average value, E^*, were computed. In the xy plane, the behavior of the A_3D and B_3D structures is symmetrical, while the structures C_3D and D_3D are anisotropic. Despite the simplification adopted, the 2D structures reflect the behaviour of the corresponding 3D structures, as evidenced by the ratio between the apparent elastic moduli in the x and in the y directions reported in Tab.1.

Table 1: Ratio between the apparent elastic moduli E_x^* and E_y^* of each structure in the 3D and in the 2D models.

E_x^*/E_y^*	A	B	C	D
3D	1.0	1.0	1.2	1.5
2D	1.0	1.0	1.1	1.4

The correlation coefficient between the values of the apparent elastic moduli $E^*(3D)$, computed from the three-dimensional structures, and the $E^*(2D)$, computed from the planar models, is very high, $R^2 = 0.994$, Fig.8. As expected, the numerical values of the average apparent elastic moduli E^* are not the same for the 3D and of the 2D structures, but the goal of the present research is to establish a tool for ranking the trabecular configurations on the basis of their ability to withstand the applied loads, there is no need to assess the exact value of the bone elastic modulus. The relative changes between the parameters computed for different structures provide a suitable indicator to express the ability of a parameter to classify the trabecular arrangements.

In Tab. 2 it can be appreciated how the apparent elastic modulus maintains the ability to differentiate among the structures in the transition from 3D to 2D.

Table 2: Ratios of the average apparent elastic moduli E^* computed for the different structures.

	E_A^*/E_B^*	E_A^*/E_C^*	E_A^*/E_D^*
3D	4.3	4.7	5.2
2D	4.3	4.4	5.3

Tab. 3 shows the values of the ratio between the 3D and the 2D mineralization factor, CF, again with respect to the A configuration. As already mentioned, the 3D and 2D *CF* have the same numerical values. The ratios shown in Table 3 confirm
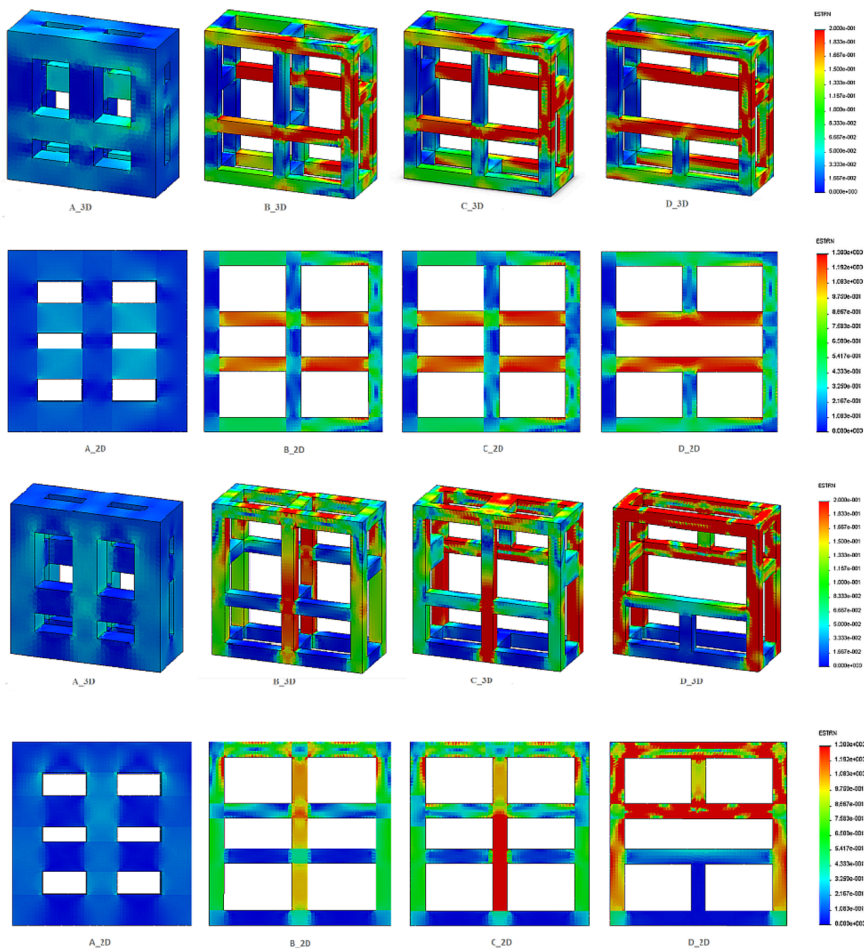
Figure 5: Distribution of equivalent strain intensity: (a) 3D models, compression along the *x* axis; (b) 2D models, compression along the *x* axis; (c) 3D models, compression along the *y* axis; (d) 2D models, compression along the *y* axis.

that density measurements are not able to grasp the different mechanical behaviour of configurations of equal apparent density, like the B and C structures.

Finally, the ratios of the Structure index *SI* were computed for the 2D models, as reported in Tab. 4. Not only this index is able to rank the various structures, but it is even able to emphasize the differences among structures more clearly than the 3D apparent elastic modulus, highlighting the influence of the spatial organization of the trabeculae on the elastic behavior of the bone and its ability to withstand the loads.
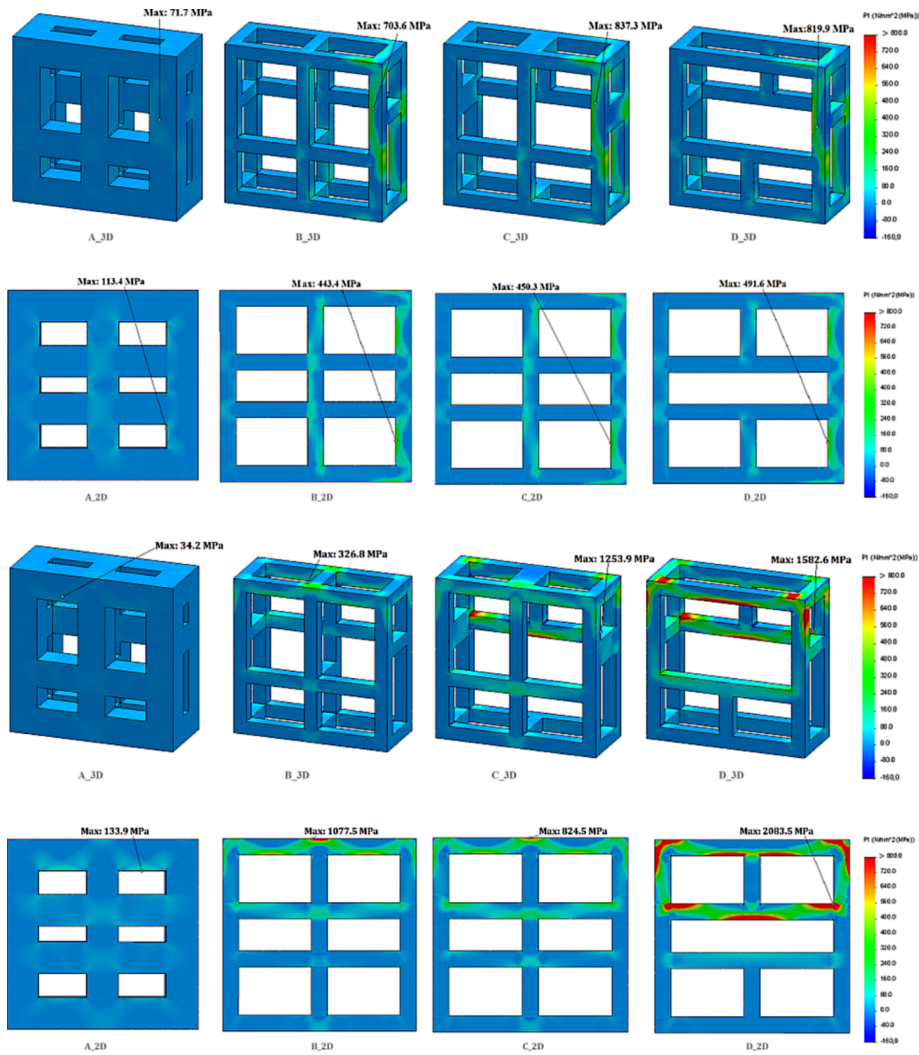
Figure 6: Distribution of first principal stress intensity: (a) 3D models, compression along the *x* axis; (b) 2D models, compression along the *x* axis; (c) 3D models, compression along the *y* axis; (d) 2D models, compression along the *y* axis.

Table 3: Ratios of the mineralization factor *CF* in the different structures. The *CF* values coincide in the corresponding 3D and 2D configurations.

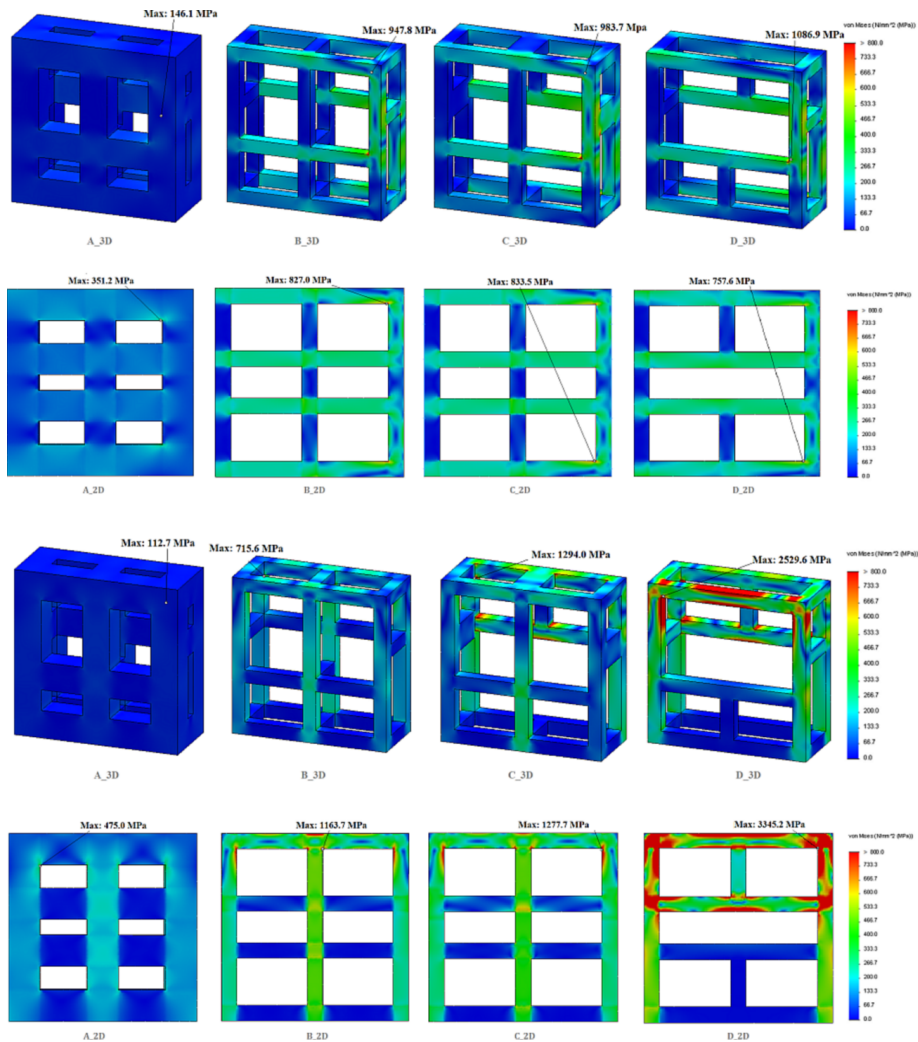|	CF_A/CF_B	CF_A/CF_C	CF_A/CF_D
3D	3.06	3.06	3.55
2D	3.06	3.06	3.55

Figure 7: Distribution of Von Mises stress intensity: (a) 3D models, compression along the *x* axis; (b) 2D models, compression along the *x* axis; (c) 3D models, compression along the *y* axis; (d) 2D models, compression along the *y* axis.

5 Discussion

Indications that there is a close relation between changes in hand trabecular bone structure and fracture-relevant skeletal sites can be found in literature. Bone mineral density can be measured by digital X-ray radiogrammetry at peripheral hand bones (e.g. phalanxes, metacarpus, or three middle metacarpal bones) and be re-
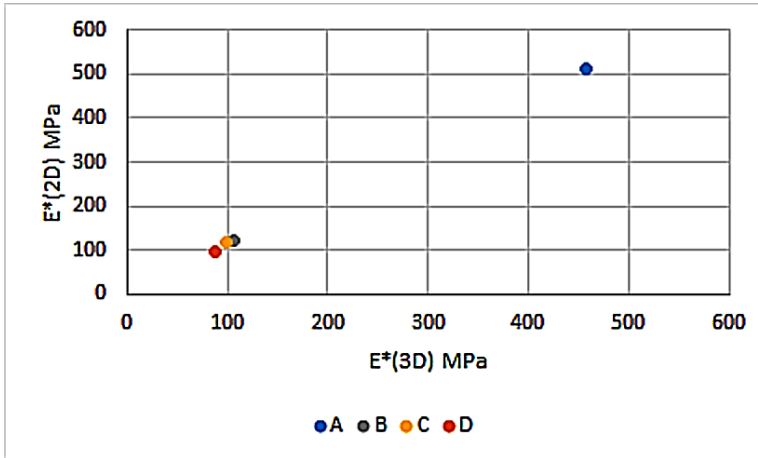
Figure 8: Average value of the apparent elastic modulus in the directions of controlled displacement computed for the planar models, $E^*(2D)$, and for the three-dimensional structures, $E^*(3D)$, $R^2 = 0.994$.

Table 4: Ratios of the structure index *SI* in the different 2D models.

	SI_A/SI_B	SI_A/SI_C	SI_A/SI_D
3D	13.3	19.1	35.7

lated to the values obtained by dual energy X-ray absorptiometry in the femoral neck, [46,47,48,49,50]. Moreover, several studies have demonstrated that quantitative ultrasound (QUS) measurements performed at the first phalanx of the hand fingers can be used to assess the individual risk of fracture and are able to detect age-related alterations in bone tissue with a diagnostic sensitivity equal to that of lumbar densitometry, when used for discriminating between women with or without osteoporotic vertebral fractures [51,52,53].

The X-ray images of the bone structures of 6 female subjects, ages 35-77, were collected at CSMMO (Centro Studi Malattie Metaboliche dell'Osso, Gorizia, Italy). A clinical evaluation of the subjects was performed by a blinded independent medical specialist, by combining the risk factors usually considered in Italy at the time of data collection: age, familiarity, lumbar spine density and vertebral collapses. The results are summarized in Tab. 5, where the agreement between the *SI* value and the bone structure quality can be appreciated.

Table 5: Structure Index and clinical evaluation of six female subjects, age 35-77.

SI	Clinical evaluation
109	Full-blown osteoporosis, confirmed by the presence of multiple fragility fractures
120	Severe osteoporosis
122	Advanced osteoporosis with multiple fragility fractures
133	Light degree osteopathy, a fragility fracture argues for established osteoporosis
222	Healthy subject to be monitored for familiarity to fragility fractures and a T-score next to -1 despite her young age
259	Healthy person at no particular risk

6   Conclusions

The positive results obtained indicate that the Structure Index is able to differentiate among the idealized structures despite the loss of information due to the use of a 2D radiographic images, highlighting the relevance of this Cell Method application in the evaluation of trabecular bone elastic quality alterations due to changes in the trabecular structure quality.

The high social costs of osteoporosis and the difficulties encountered in clinical practice when addressing the issue of assessing the patient fracture risk, compared to the very low costs of the test and the wide availability of the necessary equipment, make the *SI* a highly promising tool for the early diagnosis of osteoporotic diseases and screening, for monitoring the clinical evolution and/or the response to specific therapies (follow-up) and, in general, for making an accurate assessment of bone alterations due to age, pathological conditions and lack of exposure to physiological mechanical stimuli, as encountered in micro-gravity conditions.

G. Mazzoleni for support to the development of this project.

References

1. Johnell, O. & Kanis, J. A. (2006) An estimate of the worldwide prevalence and disability associated with osteoporotic fractures. *Osteoporosis Int.*, 17, 12, 1726-1733.

2. World Health Organization Scientific Group (2008) *Assessment of osteoporosis at the primary health-care level*. Available at http://www.who.int/chp/topics/ Osteoporosis.pdf Accessed March 23, 2015.

3. Kanis, J. A., Johnell, O., Oden, A., Sembo, I., Redlund-Johnell, I., Dawson, A., De Laet, C. & Jonsson, B. (2000) Long-term risk of osteoporotic fracture in Malmo. *Osteoporos Int.,* 11, 8, 669-674.

4. Melton, L. J. 3rd, Chrischilles, E. A., Cooper, C., Lane, A. W. & Riggs, B. L. (1992) Perspective how many women have osteoporosis? *J. Bone Miner. Res.*, 7, 1005–1010.

5. Melton, L. J. 3rd, Atkinson, E. J., O'Connor, M. K., O'Fallon, W. M. & Riggs, B. L. (1998) Bone density and fracture risk in men. *J. Bone Miner Res.*, 13, 12, 1915-1923.

6. Cooper, C., Atkinson, E. J., Jacobsen, S. J., O'Fallon, W. M. & Melton, L. J. 3rd (1993) Population-based study of survival after osteoporotic fractures. *Am. J. Epidemiol.*, 137, 9, 1001-1005.

7. National Osteoporosis Foundation *Clinician's Guide to Prevention and Treatment of Osteoporosis*. Available at http://nof.org/files/nof/public/content/file/ 344/upload/159.pdf Accessed April 20, 2015.

8. Michel, J. P., Hoffmeyer, P., Klopfenstein, C., Bruchez, M., Grab, B. & d'Epinay, C. L. (2000) Prognosis of functional recovery 1 year after hip fracture: typical patient profiles through cluster analysis. *J. Gerontol A Biol Sci. Med. Sci.*, 55, 9, M508-M515.

9. Trombetti, A., Herrmann, F., Hoffmeyer, P., Schurch, M. A., Bonjour, J. P. & Rizzoli, R. (2002) Survival and potential years of life lost after hip fracture in men and age-matched women. *Osteoporosis Int.*, 13, 9, 731-737.

10. Freedman, K. B., Kaplan, F. S., Bilker, W. B., Strom, B. L. & Lowe, R. A. (2000) Treatment of osteoporosis: are physicians missing an opportunity? *J. Bone Joint Surg. Am.*, 82, 8, 1063-1063.

11. Siris, E. S., Miller, P. D., Barrett-Connor, E., Faulkner, K. G., Wehren, L. E., Abbott, T. A., Berger, M. L., Santora, A. C. & Sherwood, L. M. (2001) Identification and fracture outcomes of undiagnosed low bone mineral density in postmenopausal women: results from the National Osteoporosis Risk Assessment. *JAMA.*, 286, 22, 2815-2822.

12. Pasco, J. A., Seeman, E., Henry, M. J., Merriman, E. N., Nicholson, G. C., Kotowicz, M. A. (2006) The population burden of fractures originates in women with osteopenia, not osteoporosis. *Osteoporos. Int.*, 17, 9, 1404-1409.

13. Siris, E. S., Chen, Y. T., Abbott, T. A., Barrett-Connor, E., Miller, P. D., Wehren, L. E., Berger, M. L. (2004) Bone mineral density thresholds for pharmacological intervention to prevent fractures. *Arch. Intern. Med.*, 164, 1108 – 1112.

14. Sornay-Rendu, E., Munoz, F., Garnero, P., Duboeuf, F. & Delmas, P. D. (2005) Identification of osteopenic women at high risk of fracture: the OFELY study. *J. Bone Miner. Res.*, 20, 10, 1813-1819.

15. Szulc, P., Munoz, F., Duboeuf, F., Marchand, F. & Delmas, P. D. (2005) Bone mineral density predicts osteoporotic fractures in elderly men: the MINOS study. *Osteoporosis Int.*, 16, 19, 1184-1192.

16. Wainwright, S., Phipps, K. & Stone, J. (2001) A large proportion of fractures in postmenopausal women occur with baseline bone mineral density t-score – 2.5. *J. Bone Miner. Res.*, 16, S155.

17. Friedman, A. W. (2006) Important determinants in bone strength: beyond bone mineral density. *J. Clin. Rheumatol.*, 12, 70-77.

18. Kanis, J. A., Johnell, O., Oden, A., Johansson, H. & McCloskey, E. (2008) FRAX and the assessment of fracture probability in men and women from the UK. *Osteoporosis Int.*, 19, 4, 385-397.

19. Jones, G., Nguyen, T., Sambrook, P. N., Kelly, P. J., Gilbert, C. & Eisman, J. A. (1994) Symptomatic fracture incidence in elderly men and women: The Dubbo osteoporosis epidemiology study (DOES). *Osteoporosis Int.*, 4, 5, 277-282.

20. Kleerekoper, M., Villanueva, A. R., Stanciu, J., Rao, D. S., Parfitt, A. M. (1985) The role of three dimensional trabecular microstructure in the pathogenesis of vertebral compression fractures. *Calcif Tissue Int.*, 37, (Suppl), S594–S597.

21. Consensus Development Conference (1993) Diagnosis, prophylaxis and treatment of osteoporosis. *AM J Med.*, 94, 646-650.

22. Barou, O., Valentin, D., Vico, L., Tirode, C., Barbier, A., Alexandre, C. & Lafage-Proust, M. H. (2002) High-resolution three-dimensional micro-computed tomography detects bone loss and changes in trabecular architecture early: comparison with DEXA and bone histomorphometry in a rat model of disuse osteoporosis. *Invest Radiol.*, 37, 40-46.

23. Ruppel, M. E., Miller, L. M. & Burr, D. B. (2008) The effect of the microscopic and nanoscale structure on bone fragility. *Osteoporos. Int.*, 19, 1251-1265.

24. Liu, X. S., Zhang, X. H., Guo, X. E. (2009) Contributions of trabecular rods of various orientations in determining the elastic properties of human vertebral trabecular bone. *Bone.*, 45, 1, 158–163.

25. Yeni, Y. N., Kim, D. G., Divine, G. W., Johnson, E. M. & Cody, D. D. (2009) Human cancellous bone from T12–L1 vertebrae has unique microstructural and trabecular shear stress properties. *Bone.*, 44, 1, 130–136.

26. Haïat, G., Padilla, F., Svrcekova, M., Chevalier, Y., Pahr, D., Peyrin, F., Laugier, P. & Zysset, P. (2009) Relationship between ultrasonic parameters and apparent trabecular bone elastic modulus: A numerical approach. *J. Biomech.*, 42, 13, 2033-9.

27. Cosmi, F. (2008) *Method to identify the mechanical properties of a material*. Patent US-10509512, deposited by University of Trieste.

28. Cosmi, F. & Dreossi, D. (2007a) The Application of the Cell Method in a Clinical Assessment of Bone Fracture Risk. *Acta of Bioengineering and Biomechanics*, 9, 1, 35-39.

29. Cosmi, F. & Mazzoleni, G. (2014) Evaluation of the structural quality of bone in a case of progressive osteoporosis complicating a CRPS syndrome of the upper limb. *J. Mech. Behav. Biomed. Mater.,* 29, 517-528.

30. Tonti, E. (2001) A Direct Discrete Formulation of Field Laws: The Cell Method. *CMES: Computer Modeling in Engineering & Sciences*, 2, 1, 237-258.

31. Cosmi, F. & Di Marino, F. (2001) Modelling of the Mechanical Behaviour of Porous Materials: A New Approach. *Acta of Bioengineering and Biomechanics*, 3, 55-66.

32. Tonti, E. & Zarantonello, F. (2009) Algebraic Formulation of Elastostatics: the Cell Method. *CMES: Computer Modeling in Engineering & Sciences*, 39, 3, 201-236.

33. Pani, M. & Taddei, F. (2013) The Cell Method: Quadratic Interpolation with Tetrahedra for 3D Scalar Fields. *CMES: Computer Modeling in Engineering & Sciences*, 94, 4, 279-300.

34. Tonti, E. (2014) Why starting from differential equations for computational physics? *Journal of Computational Physics*, 257B, 1260–1290.

35. Roux, S. (1990) Continuum and Discrete Description of Elasticity. In: H.J. Herrmann and S. Roux (ed.) *Statistical Models for the Fracture of Disordered Media*, Elsevier, North Holland, 109-113.

36. Cosmi, F. (2004) Two-dimension estimate of effective properties of solid with random voids. *Theoretical and Applied Fracture Mechanics*, 42, 183-186.

37. Cosmi, F. (2011a) A Cell Method model for sintered alloys. *CMES: Computer Modeling in Engineering & Sciences*, 74, 3-4, 269-282.

38. Cosmi, F. & Bernasconi, A. (2010) Elasticity of short fibre reinforced polyamide: morphological and numerical analysis of fibre orientation effects. *Materials Engineering*, 2, 6-10.

39. Cosmi, F. (2011b) Local anisotropy and elastic properties in a short glass fibre reinforced polymer composite. *Strain*, 47, 215–221.

40. Cosmi, F. (2011c) A micro-mechanical model of the elastic properties of a short fibre reinforced polyammide. *Procedia Engineering*, 10, 2135-2140.

41. Cosmi, F. & Dreossi, D. (2007b) Numerical and experimental structural analysis of trabecular architectures. *Meccanica*, 42, 1, 85-93.

42. Taddei, F., Pani, M., Zovatto, L., Tonti, E. & Viceconti, M. (2008) A new meshless approach for subject-specific strain prediction in long bones: Evaluation of accuracy. *Clinical Biomechanics*, 23, 1192-1199.

43. Cosmi, F., Steimberg, N., Dreossi, D. & Mazzoleni, G. (2009) Structural analysis of rat bone explants kept in vitro in simulated microgravity conditions. *J. Mech. Behav. Biomed. Mater.*, 2, 1, 164-172.

44. Currey, J. (2002) *Bones, structure and mechanics*. Princeton University Press, Woodstock.

45. Zioupos, P., Cook, R. B. & Hutchinson, J. R. (2008) Some basic relationships between density values in cancellous and cortical bone. *J Biomech.*, 41, 1961–1968.

46. Wilczek, M. L., Kälvesten, J., Algulin, J., Beiki, O., Brismar, T. B. (2013) Digital X-ray radiogrammetry of hand or wrist radiographs can predict hip fracture risk—a study in 5,420 women and 2,837 men. *Eur Radiol.,* 23, 1383–1391.

47. Dhainaut, A., Rohde, G., Hoff, M., Syversen, U. & Haugeberg, G. (2011) Phalangeal densitometry compared with dual energy X-ray absorptiometry for assessment of bone mineral density in elderly women. *J. Womens Health (Larchmt).*, 20, 12, 1789-1795.

48. Friis, M. (2001) Digital X-ray Radiogrammetry on Hand X-rays Obtained on Mammographic X-ray Equipment. *J. Int. Bone and Mineral Society*, 28, 5(suppl), P336.

49. Rosholm, A., Hyldstrup, L., Backsgaard, L., Grunkin, M., Thodberg, H. H. (2001) Estimation of bone mineral density by digital X-ray radiogrammetry: theoretical background and clinical testing. *Osteoporos. Int.*, 12, 11, 961-969.

50. Jørgensen, J. T., Andersen, P. B., Rosholm, A. & Bjarnason, N. H. (2000) Digital X-ray radiogrammetry: a new appendicular bone densitometric method with high precision. *Clin Physiol.*, 20, 5, 330-335.

51. Albanese, C. V., De Terlizzi, F., Passariello, R. (2011) Quantitative ultrasound of the phalanges and DXA of the lumbar spine and proximal femur in evaluating the risk of osteoporotic vertebral fracture in postmenopausal women. *Radiol Med.*, 116, 1, 92-101.

52. Alenfeld, F. E., Wüster, C., Funck, C., Pereira-Lima, J. F., Fritz, T., Meeder, P. J., Ziegler, R. (1998) Ultrasound Measurements at the Proximal Phalanges in Healthy Women and Patients with Hip Fractures. *Osteoporosis Int.*, 8, 5, 393-398.

53. Mele, R. (1997) Three-year longitudinal study with quantitative ultrasound at the hand phalanx in a female population. *Osteoporos Int.*, 7, 6, 550-557.